Depth-dependent investigation of defects and impurity doping in GaN/sapphire using scanning electron microscopy and cathodoluminescence spectroscopy

X. L. Sun and S. H. Goss
Department of Electrical Engineering, Ohio State University, 205 Dreese Lab, 2015 Neil Avenue, Columbus, Ohio 43210

L. J. Brillson
Department of Electrical Engineering, Center for Materials Research, and Department of Physics, Ohio State University, 205 Dreese Lab, 2015 Neil Avenue, Columbus, Ohio 43210

D. C. Look
Semiconductor Research Center, Wright State University, Dayton, Ohio 45435

R. J. Molnar
Lincoln Laboratory, Massachusetts Institute of Technology, Lexington, Massachusetts 02420

(Received 3 August 2001; accepted for publication 2 January 2002)

Cathodoluminescence (CL) imaging and temperature-dependent cathodoluminescence spectroscopy (CLS) have been used to probe the spatial distribution and energies of electronic defects near GaN/Al_2O_3 interfaces grown by hydride vapor phase epitaxy (HVPE). Cross sectional secondary electron microscopy imaging, CLS, and CL imaging show systematic variations in defect emissions with a wide range of HVPE GaN/sapphire electronic properties. These data, along with electrochemical capacitance–voltage profiling and secondary ion mass spectrometry provide a consistent picture of near-interface doping by O out-diffusion from Al_2O_3 into GaN over hundreds of nanometers. Low-temperature CL spectra exhibit a new donor level at 3.447 meV near the interface for such samples, characteristic of O impurities spatially localized to the nanoscale interface. CLS emissions indicate the formation of amorphous Al–N–O complexes at 3.8 eV extending into the Al_2O_3 near the GaN/sapphire interface. CLS and CL images also reveal emissions due to excitons bound to stacking faults and cubic phase GaN. The temperature dependence of the various optical transitions in the 10–300 K range provides additional information to identify the near interface defects and impurity doping.
[DOI: 10.1063/1.1454187]

I. INTRODUCTION

The group III-nitrides are attractive materials for optoelectronic devices such as GaN-based lasers, light-emitting diodes[1] and ultraviolet photodetectors,[2] and high temperature, high power electronic devices.[3] Present and future applications of GaN-based devices require the further development of the materials technology as well as the physical understanding of the materials involved. Epitaxial growth of GaN by hydride vapor epitaxy (HVPE) was developed in the 1960s.[4] Thick, bulk-like HVPE material is suitable for studies of GaN's physical properties, as well as acting as a lattice-matched substrate for device epilayers grown by metal–organic chemical vapor deposition (MOCVD)[5] and molecular beam epitaxy (MBE). However, electronically active defects within this material are poorly understood, for instance, the nature of the residual acceptor and donor[6,7] and the identification of various emissions related to defects.[8]

The states localized at the interface of GaN/sapphire can be of significant concern for certain device applications. In particular, degenerate doping and high conductance[9,10] can occur near this interface with sapphire, potentially affecting lateral transport in the overgrown device. Hence, impurity diffusion, interface reaction, and related defect formation are important to understand and control. The physical origin of the donors has until now been unclear since it may involve: (i) impurities substrate out-diffusion[11–13] or the initial growth surface, (ii) native defects induced by substrate out-diffusion or the initial growth surface, (iii) morphological structural effects, and (iv) gas phase impurities. In order to determine the physical nature of these dopants and defects, we used temperature-dependent (10–300 K) electron-excited luminescence spectroscopy in an ultrahigh vacuum (UHV) scanning electron microscope (SEM) to measure defect emissions from GaN/Al_2O_3 junctions with sheet carrier densities that varied over two orders of magnitude. We carried out cross sectional secondary electron (SE) imaging, cathodoluminescence spectroscopy (CLS), and CL imaging of these interfaces. We used electrochemical capacitance–voltage (ECV) profiling to measure epitaxial sheet carrier densities N_{int} localized near the junctions. Depth-dependent CLS and CL images provide information for detecting the location and physical origin of defects and impurity doping at GaN/Al_2O_3 interfaces. This study focuses on the spectral variations of defects and doping features as a function of depth to the interface. Our aim is to establish the nature of the optical

transitions due to defects and impurity doping in GaN/Al_2O_3, especially near interfaces.

II. EXPERIMENTS

The HVPE GaN epitaxy layers deposited on *c*-plane sapphire were obtained from several sources, designated A (A_1,A_2), B, and C. These layers had sheet interface concentrations, as determined from low-temperature Hall-effect measurements, of 6, 16, 98, and 508×10^{14} cm^{-2}, for A_1, A_2, B, and C, respectively, designated as "low" (for A_1 and A_2), "medium," and "high." Source A material incorporated a ZnO buffer layer prior to GaN growth, whereas the others did not. The ZnO layer was sputter deposited to prepare the sapphire substrate for GaN growth and was thermally desorbed before epitaxial growth.[14] A modified JEOL 7800F SEM Auger microprobe (base pressure 8×10^{-11} Torr) fitted with an Oxford Scientific monochromator with a resolution of 0.5 nm, liquid He cold stage, and visible-UV sensitive photomultiplier tube provided CL spectra and images. All windows and lenses were UV transparent. Spectra were corrected for the transmission and detection efficiency of the optical transmission. We produced cross sections by scoring the sapphire and cleaving between glass cover slips. The room temperature secondary electron image (SEI) and CLS measurement were taken using an electron beam energy of 15 keV and current of 100 pA over an area of one μm^2. For the low temperature experiments, the incident electron beam energy was 5 keV and current was 1 nA over an area less than 0.5×0.5 μm^2 raster square area. Due to the acceleration voltage, excitation occurred ~160 nm below the surface to minimize any surface artifacts. Depth-dependent CL spectra were taken as a function of the distance (d_{int}) from the GaN/Al_2O_3 interface.

III. LOW SHEET CARRIER CONCENTRATION

CL spectra of low sheet carrier concentration (N_{int}) GaN display large variations in deep level and near band edge (NBE) emissions as a function of distance from the interface. SE images of the sample cross sections provide spatial detail of the semiconductor and substrate boundaries.[15] Similar variations are evident for all of the samples studied. These room temperature data also illustrate the experimental method used to measure optical emissions versus distance for all the samples. Figure 1 illustrates the SE image of an HVPE-grown GaN/Al_2O_3 cross section (sample A_1). The dark area at the lower right corresponds to the sapphire substrate, whereas the bright line at the upper left indicates the free GaN surface. The bright area in the upper left is the sample holder. The striations extending across the GaN thickness are due to cleavage steps but have little effect on the CL spectra obtained with bulk sensitive electron beam energies of 5–15 keV. The numbered dots shown in Fig. 1 indicate the positions at which CL spectra were acquired. The number on each side of every point in Fig. 1 indicates the distance (d_{int}) from the GaN/sapphire interface in microns. The negative values refer to positions within the sapphire. From the variation in intensities with distance from the interface, it was possible to generate profiles for each CL spectral feature relative to distance from the interface. Figure 2 illustrates the intensity profiles for each of the luminescence features measured versus distance from the GaN/sapphire interface. The inset to Fig. 2 displays a typical room temperature CL spectrum for the HVPE GaN/Al_2O_3 sample interface, showing peak features at 3.8, 3.4, 2.95, and 2.2 eV. (Note that the 1.7- and 1.9-eV lines are just second-order transitions while the sharp peak at 1.78 eV is Cr emission from sapphire.) The 3.4, 2.95, and 2.2 eV features correspond to well-known emissions of the GaN near band edge (NBE), blue luminescence (BL), and yellow luminescence (YL), respectively.

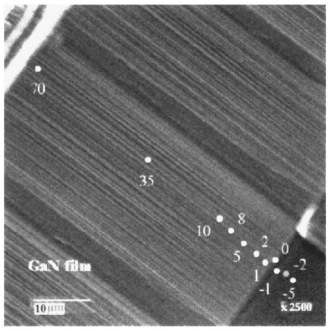

FIG. 1. Secondary electron image of the GaN film grown by HVPE on sapphire. The sapphire substrate is the dark region in the lower right corner of the image. Each dot on the SEM image represents an area where a CL spectrum was taken.

As the inset of Fig. 2 shows, the NBE, YL, 3.8, and BL peaks exhibit Gaussian line shapes in log scale spectra at the energies shown. Their relative peak intensities appear as a function of raster center distance d_{int} from the interface in

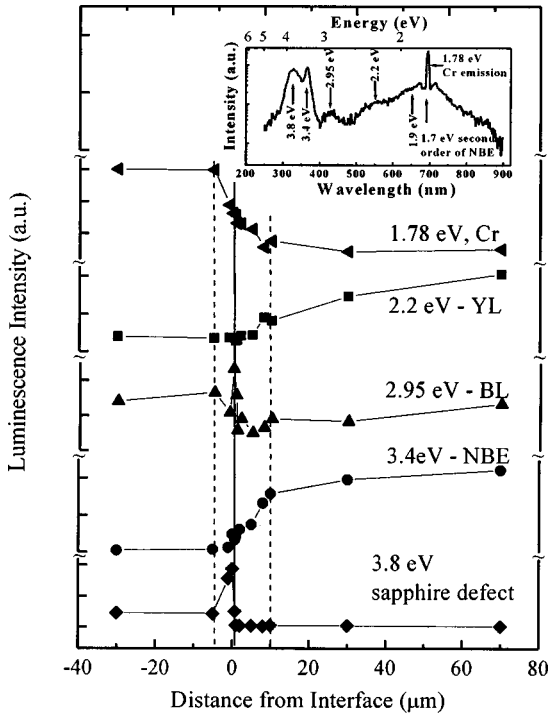

FIG. 2. CL intensity profiles for each spectral feature vs distance d_{int} from the interface. The scans are not normalized to a constant value. The GaN/sapphire interface is referenced as $d_{int}=0$.

Fig. 2. The GaN NBE emission increases rapidly within the first 10 μm from the interface into the GaN bulk, then gradually over the next 60 μm. The YL emission shows a more gradual increase with d_{int} over the same depth range. Significantly, the absolute YL intensity and its value normalized to the GaN NBE intensity both increase while dislocation density decreases with increasing $d_{int} > 10$ μm. This result suggests that dislocations are not the source of YL in the "bulk" region as proposed elsewhere.[16] The low YL intensity for $d_{int} < 2$ μm may be due to competing recombination pathways, e.g., via impurity levels. Cr emission at 1.78 eV from the Al_2O_3 decreases rapidly within this $d_{int} < 10$ μm. The 3.8 eV peak has low intensity within the Al_2O_3, increases with interface proximity, then disappears in the GaN. We argue that this peak may be due to Al–N–O complexes, since 3.8 eV emission in AlN has been assigned to O impurities.[17] A similar broad emission above band edge with different energy was observed in sample C, which will be discussed later. The broad 2.9 eV BL intensity is negligible within the Al_2O_3 or the bulk GaN but is observed for $d_{int} < 0.2$ μm. Unlike the 2.9 eV emission commonly reported for heavily Mg-doped *p*-type GaN, ours appears in an *n*-type sample. Pankove *et al.*[18] have reported broad 2.9 eV CL emission for Zn-doped GaN. Interfacial Zn might be plausible since sample A employed a ZnO buffer on the Al_2O_3. Such treatment can result in a Zn-spinel structure[19] and residual Zn impurities near the interface even though the ZnO was thermally desorbed prior to growth. However, other *n*-type samples not treated with Zn displayed 2.9 eV emission at the interface. Previous work has suggested as yet unidentified point defects and impurities as an alternative explanation for this blue emission.[20] More recent work provides evidence to correlate broad ~2.8 eV emission to the presence of O, in particular a transition from a substitutional oxygen donor (O_N) level to the $V_{Ga}-O_N$ complex acceptor.[21]

In order to identify the source of near-interface doping and defects, we obtained low temperature (10 K) CLS and CL images in a cross section of a 5 μm-thick sample (A_2, $n_{int} = 1.6 \times 10^{15}$ e/cm^2), which was also pretreated with ZnO buffer layer. Three spectra taken at different distances from the GaN/Al_2O_3 interface of A_2 are shown in Fig. 3. Since the yellow luminescence in these samples decreases strongly at low temperature to negligible levels, we present only the emissions that are near the GaN band edge. The spectra taken in the interface region ($d_{int} = 0.3$ μm) have an extra peak above the band gap (at 3.517 eV), likely due to the free electron recombination band (FERB) at degenerate carrier concentrations. As the depth increases, the intensity of this line decreases ($d_{int} = 1$ μm), and the peak disappears near the surface ($d_{int} = 4$ μm). The spectra taken in the $d_{int} = 4$ μm region show strong neutral donor bound exciton (D^0X) emission at 3.483 eV. The full width at half maximum (FWHM) of the D^0X line is 10 meV, which indicates good crystalline quality of this sample. This line may also contain contributions from free excitons, which should have energies only about 6 meV above those of the donor-bound excitons. A peak at 3.464 eV is assigned to an exciton bound to an acceptor.[22] An emission at or slightly above 3.503 eV is also observed as a shoulder on the D^0X line. The actual peak

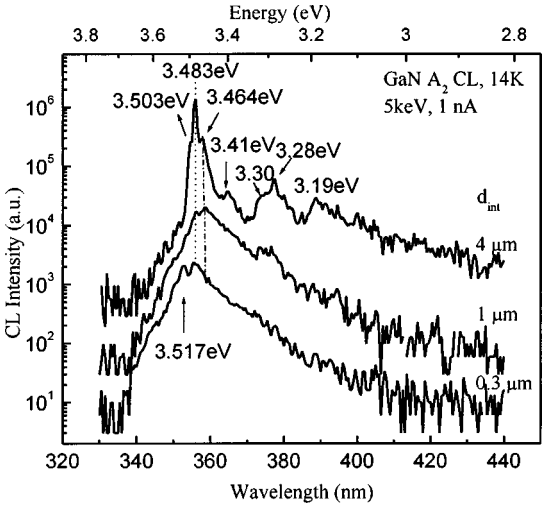

FIG. 3. CL spectra of sample A_2 acquired at $d_{int} = 0.3$, 1, and 4 μm as shown. Near-interface features differ strongly from those of the bulk.

energy may be higher than 3.503 eV, perhaps close (assuming an exciton binding energy of 26.4 meV)[23] to the expected free-exciton excited-state energy in this sample of about 3.509 eV [i.e., $3.483 + 0.006 + \frac{3}{4}(0.0264)$eV].

The CL spectra at different depths also indicate that the quality of the GaN epitaxial layer improves when the film gets thicker. However, as the d_{int} increases away from the interface, four additional optical transitions at 3.41, 3.30, 3.28, and 3.19 eV appear. The peaks at 3.28 and 3.19 eV are the characteristic neutral donor–acceptor pair recombination (D^0A^0) and its LO phonon replica (D^0A^0-LO) in the GaN bulk.

In order to understand the spatial dependence and physical nature of these peaks, we further obtained monochromatic CL images in the whole cross section of this sample at 10 K. Figure 4 shows the SEM image and the monochromatic spatial maps of some different peaks as indicated in Fig. 3. In the SEM image as shown in Fig. 4(a), the small triangle area at the lower right corresponds to the sapphire substrate, whereas the triangular region at the upper left corresponds to the free GaN surface. The arrow in each image indicates the interface. The CL image areas in Figs. 4(b) and 4(c) correspond to the same region as the SEM image. The monochromatic images display spatial variations in peak intensities at (b) 3.483 eV and (c) 3.30 eV. Textured regions within these images serve to indicate the brighter emitting areas. The luminescence intensities of some CLS peaks are weak, not well resolved, and consequently not shown here. Similarities between features within images provide an indication of optical transitions with common physical origins. However, the intensity contributions of adjacent spectral features can complicate these spatial correlations and differences between defect distributions.

Temperature-dependent (10–300 K) experiments provide additional clues to the origins of the emissions as shown in Figs. 3 and 4. Figure 5 shows the temperature-dependent spectra taken from the bulk epilayer ($d_{int} = 4$ μm). The energy of the four emissions shown all decrease with increased temperature and change at different rates. Figure 6(a) is an

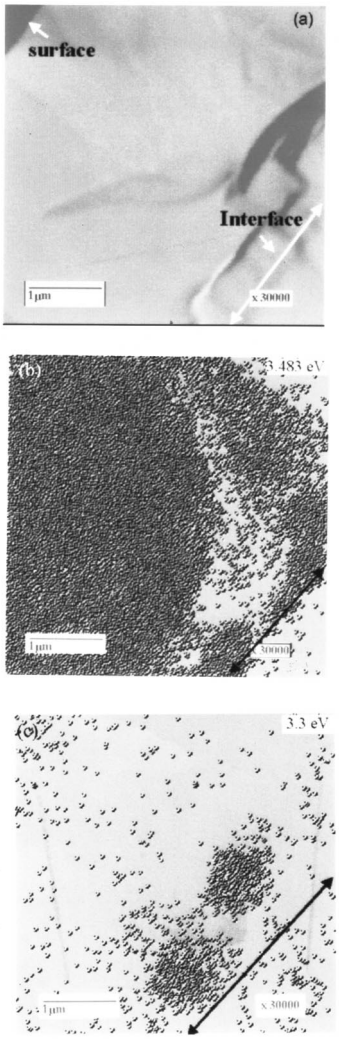

FIG. 4. (a) SEM image and CL images shown for emissions of (b) 3.483 eV and (c) 3.30 eV acquired within the cross section of sample A_2. The length scales are the same as in (a). The arrow in each CL image indicates the GaN/sapphire interface, and the numbered spots indicate where spectra were acquired.

Arrhenius plot of the integrated intensities of the D^0X peak at 3.483 eV, the 3.41-eV peak, and the 3.30 eV peak. Figure 6(b) gives the temperature dependence of their optical transition energies corresponding to Fig. 5.

The data for low N_{int} presented in Figs. 3–6 provide evidence for several near-interface phenomena. As Fig. 6(a) shows, the peak at 3.483 eV quenches first with an energy of 4 meV, then 12 meV at higher temperatures, presumably due to two competitive recombination channels. The small energy quenching of the D^0X corresponds to the thermal detrapping of exciton from the shallow donor (~6 meV) while the second nonradiative path could be ionization of the neutral donor involved in the excitonic complex.[24] These activation energies should be viewed with caution since CL intensities are affected by spectral overlap and temperature-dependent broadening.

At low temperature, the 3.41 eV is sharp and intense, indicating its excitonic nature. As temperature increases, the 3.41-eV peak in Fig. 5 becomes more pronounced and

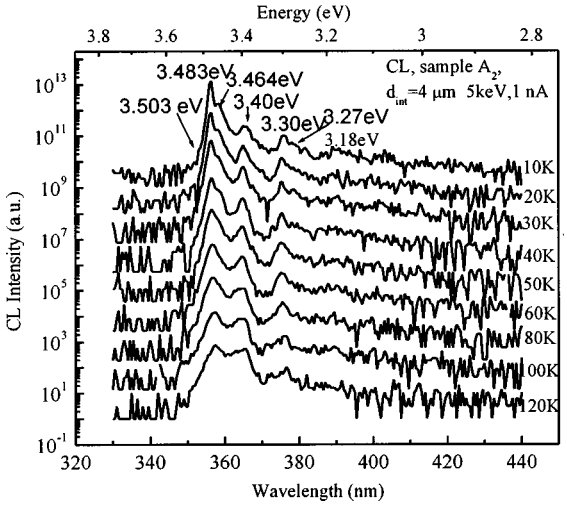

FIG. 5. Temperature dependence of the luminescence spectra of sample A_2 showing temperature quenching behaviors of each emission.

quenches very slowly. The activation energy shown in Fig. 6(a) for quenching is only 7 meV, which is lower than the activation energy for this 3.41 eV band reported by Leroux,[30] varying between 12 and 40 meV. This is because the 3.40 peak can be mixed with the LO phonon replica of the DX peak since the relative contribution of the latter increases

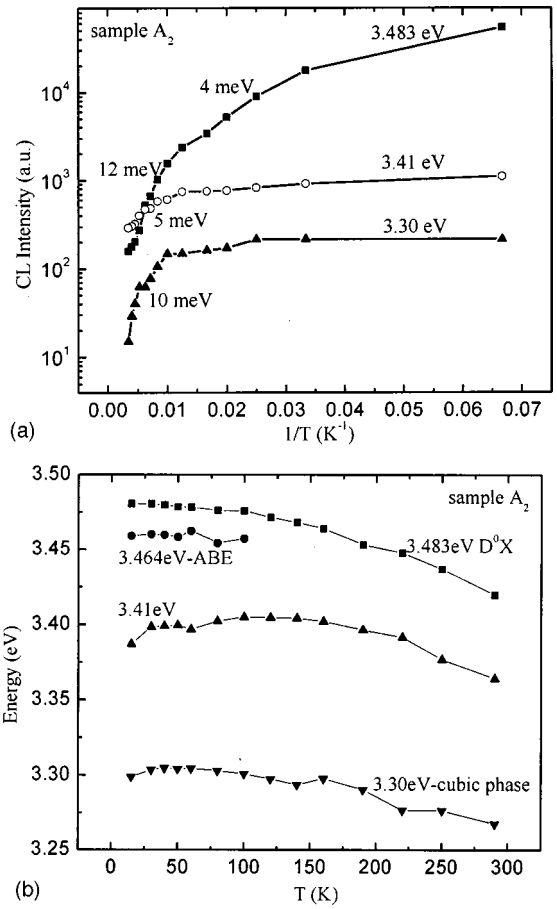

FIG. 6. (a) Temperature dependence of the 3.483, 3.41, and 3.30 eV peak intensities in Fig. 5 and (b) temperature dependence of their energies, including the 3.464 eV peak.

with temperature. A model[25] has been proposed for this frequently reported emission[26,27,28] based on recombination of an exciton bound to an I_1 type stacking fault in GaN. In this model, the stacking fault is similar to a cubic quantum well in wurtzite GaN. The electrons are trapped by the stacking fault and holes in the wurtzite matrix type II quantum well. Calleja *et al.*[29] reported a broad emission centered at 3.41 eV and attributed it to structural defects at the column/substrate interface. Combining these two models, it is not unexpected that stacking faults appear at the column/substrate interface where high density defects concentrate.

All the quenching energies reported here are lower than those of the MOCVD samples measured by photoluminescence (PL) reported by Leroux *et al.*[30] In that work, the activation energies reported for D^0X were 5–7 meV at low temperatures and 34–36 meV at higher temperatures, while the activation value for the 3.41 eV peak was 12 meV. The small value of the activation energy is probably caused by overlap and temperature-related broadening of the peaks.

The 3.30-eV peak is most prominent at $d_{\text{int}} = 1-1.5\ \mu$m as shown in Fig. 4(c) and may be indicative of another phase besides wurtzite GaN in this region. As shown in Fig. 6(a), the 3.30-eV peak quenches with an energy of 10 meV, versus 5 meV for the 3.41 eV peak at low temperatures. Furthermore, there appear to be no phonon replicas increasing with increasing temperature in Fig. 5. Hence the 3.30 eV peak is not likely to be a phonon replica of the 3.41 eV peak. Instead, we believe it is related to a second phase. From its energy, it could be due to either ZnO or cubic phase GaN domains that often coexist with the hexagonal phase. Considering that this sample was treated with a ZnO buffer layer, a ZnO phase is not unexpected close to the interface. Since secondary mass ion spectroscopy (SIMS) shows no Zn in the samples, this peak is more likely to be a cubic domain, since stacking faults are cubic in nature.

Finally, the low N_{int} A_2 specimen data show evidence for near-interface free carriers. As shown in Fig. 3, a shoulder appears above the excited state emission line, increasing in intensity for decreasing distance from the interface. In the spectra taken near the interface ($d_{\text{int}} = 0.3\ \mu$m), this structure peaking at about 3.517 eV is well resolved. This peak may be due to band-to-band transitions, since the free-carrier concentration in this near interface range is usually high.[10,31]

IV. MIDLEVEL SHEET CARRIER CONCENTRATION

Samples with higher N_{int} provide an opportunity to identify the source of the residual near-interface doping. We have carried out low temperature (10 K) CLS as a function of d_{int} of HVPE grown GaN/Al_2O_3 with carrier concentration $N_{\text{int}} = 9.8\times10^{15}\ e/\text{cm}^2$ (sample B). CLS, CL imaging, and SIMS data of unintentionally doped GaN samples provide information at the interface. Sample B was not grown on a ZnO buffer layer. The depth profile CLS in Fig. 7 exhibits the typical sharp features found in GaN, including the D^0X transitions at 3.473–3.485 eV. For distances $>1\ \mu$m, an extra peak appears at 3.388 eV, ascribed to the phonon replica of the D^0X.[30] Another dominant feature in these spectra corresponds to neutral donor–acceptor-pair (D^0A^0) transitions at

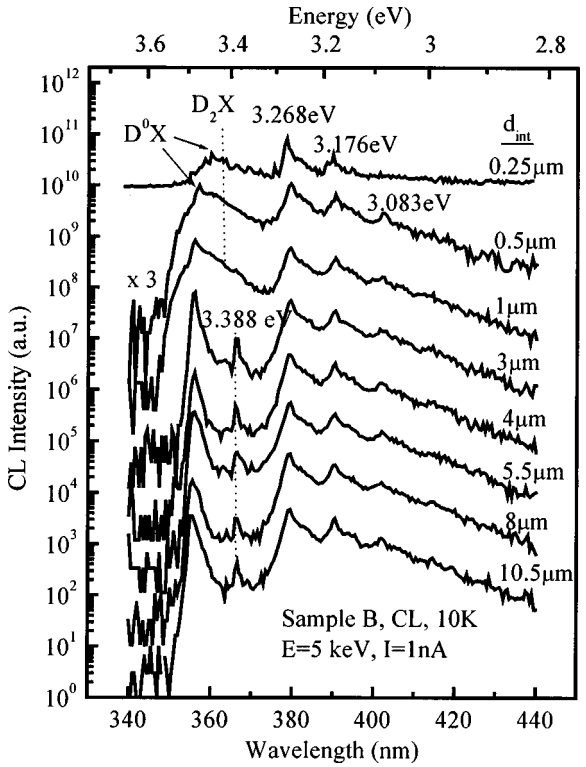

FIG. 7. Low temperature CL spectra as a function of distance from the interface. Features above and below the DX transition energy differ significantly between the interface and the bulk.

3.2 to 3.3 eV, followed by a sequence of longitudinal optical phonon replicas ($\Delta h\nu = 92$ to 93 meV). The dominant acceptor may either be C,[32] detected by SIMS in similar samples,[33,34] or the Ga vacancy, detected by positron annihilation.[34] However, it is not likely Mg, which is not detected by SIMS.[33] These features are common to GaN at all depths. However, near the interface, i.e., at $d_{\text{int}} \leqslant 1\ \mu$m, an additional feature appears at 3.447 eV, somewhat broader than the D^0X peak.

Figure 8 shows the SEM image of sample B along with monochromatic CL images taken at 10 K. CL images are shown for (b) 3.483 eV due to D^0X luminescence and (c) 3.28 eV due to D^0A^0 transitions. The emission of D^0X fluctuates in intensity, whereas the emissions of D^0A^0 are dominant and quite uniform. Figure 9 illustrates the temperature-dependent CL spectra of sample B taken at $d_{\text{int}} = 3\ \mu$m, showing the DX, D^0A^0, and phonon replicas.

The data for intermediate N_{int} presented in Figs. 7–9 illustrate significant changes from the bulk to the near-interface region. The depth dependent CL spectra show that at $d_{\text{int}} > 1\ \mu$m, D^0X has a blueshift to 3.483 eV, which is probably due to a reduction in band tailing. An important feature in the near interface region is the broadening of the exciton peaks. As d_{int} increases, the FWHM of the D^0X and D^0A^0 transitions become narrower, showing that the crystalline quality of the sample improves with distance away from the interface, up to $d_{\text{int}} = 3\ \mu$m.

An additional feature at 3.447 eV, appearing near the interface, arises from the degenerate doping. A broad structure is not unexpected in the highly degenerate region, due to

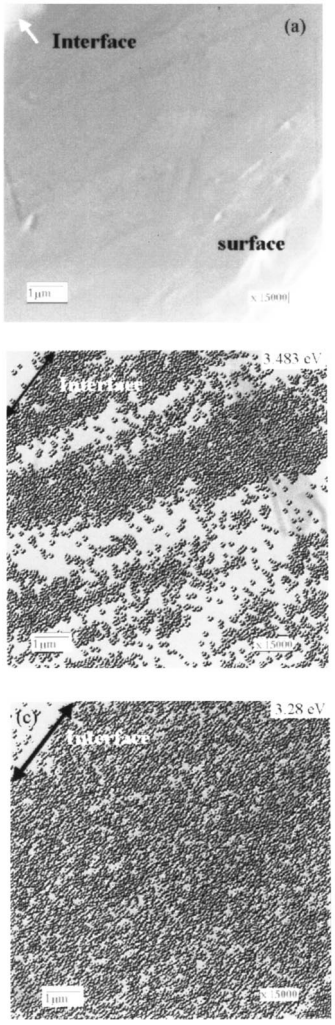

FIG. 8. Sample B SEM image in (a) and CL images for emissions in cross section at 3.483 eV in (b), and 3.28 eV in (c). The length scales are those shown in the SEM image. The arrow in each CL image indicates the GaN/sapphire interface.

band tailing and band filling (Moss–Burstein) effects or less than perfect crystal quality. However, the 3.447 eV peak may also be a two-electron replica of the D^0X line,[30] because such a line would be expected at $3.473\ \mathrm{eV}-(3/4)E_D$, where E_D should be about 30 meV. That is, the final state of the 3.473 eV transition is the ground state $(n=1)$ of the donor, whereas the 3.447 eV transition would then have an $n=2$ final state. But if this latter model were correct, then the two transitions might be expected to have about the same linewidth and the ratio between the two peaks should be more constant at the chosen temperature. However, besides the change in linewidth apparent in Fig. 7, this figure also shows that this ratio changes considerably at different depths. This behavior is therefore not consistent with a two-electron replica.

Another possibility for the 3.447-eV transition is an exciton bound to a deep donor or acceptor. If the Haynes factor is 0.1 to 0.2,[35] then this deep center would have an energy of about 150–300 meV from a band edge. An acceptor-bound exciton would be the most likely candidate, since acceptor centers are clearly evident from the strong D^0A^0 transitions.

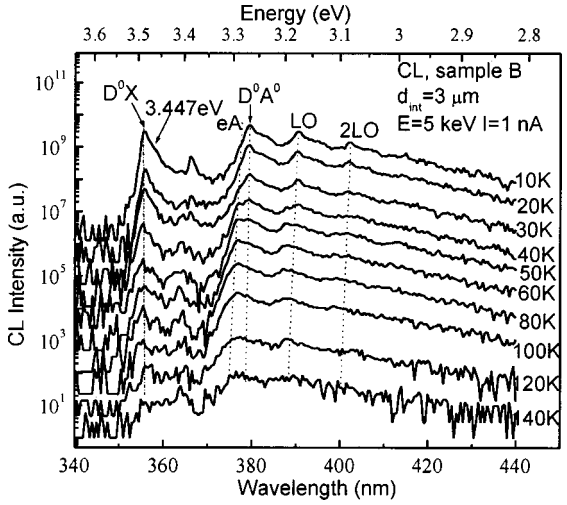

FIG. 9. Temperature dependence of the *DX*, D^0A^0, and phonon replica peak luminescence features of sample B.

Of all possible acceptors, only the Ga vacancy would have a high enough concentration, i.e., from positron annihilation spectroscopy (PAS), $[V_{Ga}]=10^{17}$ to $10^{18}\ \mathrm{cm}^{-3}$ in a MOCVD GaN epilayer,[36] or even $>10^{19}\ \mathrm{cm}^{-3}$ in HVPE GaN materials.[34] However, PAS in conjunction with Hall measurements show that V_{Ga} is the dominant acceptor everywhere, both in the interface and bulk regions,[34] while the 3.447 eV emission is only evident near the interface. Therefore the depth-dependent CLS results argue against assignment of this feature to Ga vacancies.

With regard to donors, Si and O are believed to induce a shallow donor state with a binding energy of 31 and 34–35 meV, respectively.[37] The only donor with a high enough concentration to give the observed strong intensity of the 3.447 eV peak near the interface is O, because O concentration increases strongly near the interface, whereas the concentration of Si does not.[34] Figure 10 shows SIMS measurements of this specimen performed at Chas. Evans and Associates.[33] The SIMS plot displays concentrations as high as $7\times10^{19}\ \mathrm{cm}^{-3}$ near the interface, decreasing to mid-

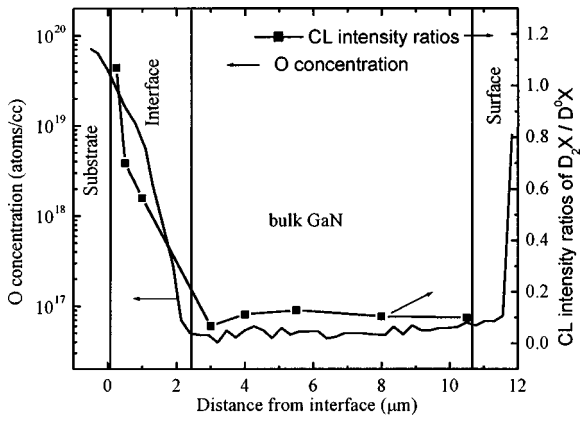

FIG. 10. O profiles near the interface detected by SIMS compared with the luminescence intensity of the 3.447 eV peak relative to the D^0X near band edge emission. The clear similarity in depth dependence demonstrates that O diffusion from the sapphire is correlated with the 3.447 eV donor level.

10^{18} cm^{-3} over a distance range $d_{int} \leqslant 1$ μm. Similarly, the ratio of the 3.447 eV transition (termed D_2X) relative to the D^0X near band edge emissions is highest at the interface and decreases steadily with distance over the same 2 μm into the GaN. Significantly, Si and C impurity concentrations in this interface region are several orders of magnitude smaller and exhibit no strong variation with depth.[33] No other donor impurity is localized in this depth range. Electron concentration n_{int} (measured by ECV) is also extremely high in the interface region. Here again, the comparison of carrier concentrations versus depth reveals a close correspondence between a shallow donor and O.[34] This agreement between optical, chemical, and electrical features indicates that electron donors in the interface region must come mainly from O. Furthermore, this identification is consistent with the assignment of interface-localized blue (2.8 to 2.9) eV luminescence in *n*-type GaN to O donor-related complexes, as discussed in Sec. III. Overall, the close correlation between CLS spectral peak intensities with [O] spatial distribution indicates that O impurities diffused from the Al_2O_3 are the origin of the high sheet carrier concentration.

At low temperature, the CL is dominated by neutral donor bound exciton (D^0X) transitions. With increasing temperature, Fig. 9 shows that the *A* free exciton line increases as the D^0X peak quenches. Other features appearing in the spectra are D^0A^0 lines near 3.27 eV and their LO and 2LO phonon replicas near 3.18 and 3.09 eV, respectively. These involve the usual residual acceptor, possibly carbon or the Ga vacancy as described before. As temperature increases, the D^0A^0 emission is replaced by band–acceptor (*eA*) emission. The latter can be distinguished from the former since it shifts to higher energy with increasing temperature. Figure 9 shows that the energy difference between *DA* and *eA* transitions is 23 meV and is in principle a measure of the background donor binding energy. We neglect the Coulomb correction in this simple approach. Including this correction effectively increases the donor binding energy. Figure 9 shows a shoulder appearing on the lower energy side of both D^0X and D^0A^0 emissions. These shoulders may be related to coupling with other than LO phonons. As shown in the CL image of D^0X in Fig. 8(b), the edge emission fluctuates in intensity and is weak at grain boundaries, i.e., in the regions of high defect density. It is likely that these regions with high defect density play a role in trapping impurities.

V. HIGH SHEET CARRIER CONCENTRATION

In this section we discuss the behavior of optical transitions in a 17 μm-GaN sample (sample C) with the highest relative N_{int} (5.0×10^{16} e/cm^2). Here the sapphire substrate was nitrided prior to deposition by exposure to NH_3. Figure 11 illustrates low temperature (10 K) CLS as a function of d_{int}, analogous to Figs. 3 and 7. The depth-dependent CLS in Fig. 11 exhibits a broadband above the band edge emission as $d_{int} \leqslant 5$ μm, labeled as X_1. As the depth increases, the spectrum is dominated by D^0X at 3.483 eV. The FWHM also decreases with thickness increasing, and the FWHM of the strongest D^0X at $d_{int}=10$ μm is 15 meV, showing that this sample has good crystal quality. For distance d_{int}

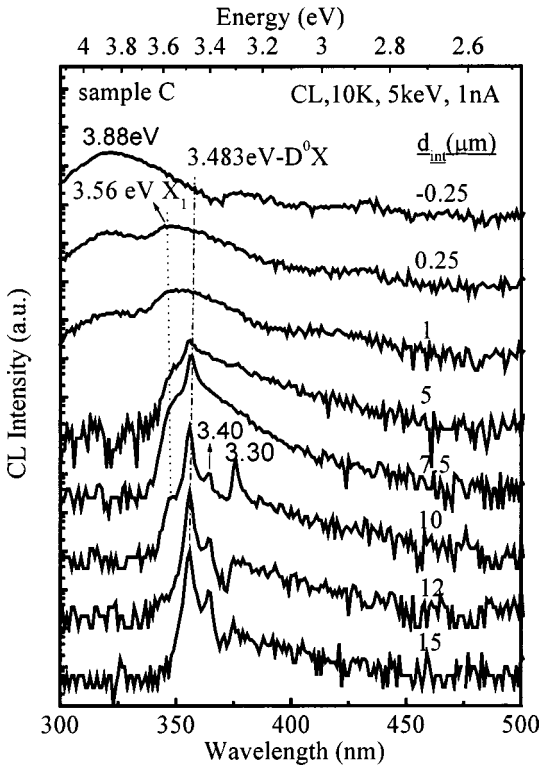

FIG. 11. Low temperature depth profile CL spectra of sample C showing emissions at 3.56, 3.483, 3.40, and 3.30 eV.

$\geqslant 10$ μm, two extra peaks at 3.40 and 3.30 eV become prominent. They are ascribed to excitons bound to stacking faults and a cubic GaN domain, respectively, as discussed in Sec. III.

We also obtained monochromatic spatial maps of the emission intensities for different spectral features within the cross sectional structure. Figure 12 shows the SEM image (a) and the monochromatic spatial maps of different peaks at (b) 3.563 eV, (c) 3.483 eV, (d) 3.40 eV, and (e) 3.30 eV. In the SEM image, the small triangular area at the lower right corresponds to the sapphire substrate, whereas the line at the upper left indicates the free GaN surface. CL images were recorded from the same region as that shown in the SEM image. Enhanced image contrast and brightness serve to highlight emitting areas and enhance comparison of features from image to image.

As shown in Fig. 11, a broadband at 3.88 eV appears at $d_{int} \leqslant 1$ μm. Just as with the 3.8-eV (at room temperature) peak in sample A_1, this feature has high intensity near the GaN/Al_2O_3 interface ($d_{int}=-0.25$–0.25 μm), but decreases into the GaN bulk. Unlike impurity band filling even for impurity concentrations $>10^{20}$ cm^{-3}, this peak is centered well above the conduction band edge and due to an amorphous Al–N–O complex. This is consistent with the increasing in peak intensity with proximity to the interface.

As shown in Fig. 11, the energy and width of the broadband X_1 changes with the thickness of the epilayer, particularly at the interface ($d_{int} \leqslant 1$ μm), where a broad feature centered at 3.56 eV appears. These spectra are typical of a highly doped material with an electron concentration of about 10^{19} cm^{-3} based on the model proposed by

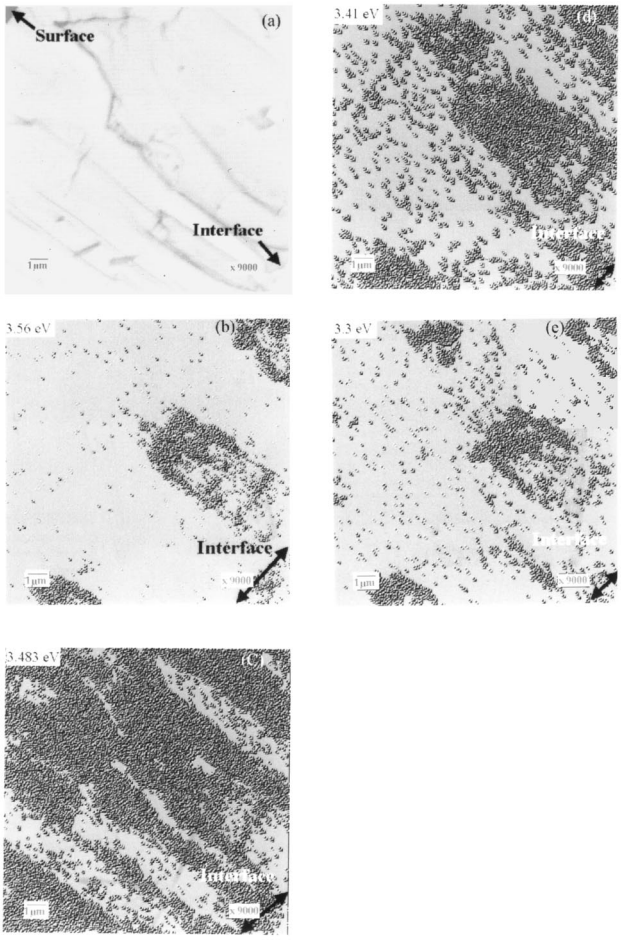

FIG. 12. (a) SEM image and CL images for emissions at (b) 3.56 eV, (c) 3.483 eV, (d) 3.41 eV, and (e) 3.30 eV. The length scales are all the same as that shown in the SEM image, and the arrow in each CL image indicates the GaN/sapphire interface.

Arnaudov.[38] The possible explanations for this broadening to higher energies are band filling at these degenerate doping levels, and the free-electron recombination across the band gap.[38] The energy of this broad emission extends to 3.6 eV, also possibly due to Al–GaN alloy. Such NBE corresponding to $Al_xGa_{1-x}N$ alloying has been previously observed at Al–GaN interfaces.[39] Pregrowth nitridation of sapphire for such specimens should further enhance Al–N bonding and alloying.[40] For samples nitrided inside the HVPE reactor at high temperature, a thin AlN layer is not unexpected, given the reaction:

$$Al_2O_3 + 2NH_3 \Rightarrow 2AlN + 3H_2O. \quad (1)$$

The formation of AlN islands as a result of a high temperature NH_3 exposure has also been reported in the literature.[40,41] This high temperature environment may also lead to desorption of H_2O and O impurities near the interface.

The image of the band edge CL emission (3.483 eV) as shown in Fig. 12(c) indicates spatial striations in intensity, indicative of columnar structure. The decrease in D^0X emission intensity between these columnar regions may be due to grain boundaries, i.e., regions of high defect density, which can act as efficient centers of nonradiative recombination. Therefore edge emission is expected to quench at grain boundaries. The CL images in Fig. 12(b) show that the X_1 peak at 3.56 eV appears in the same spatially localized regions as the 3.41 and 3.30 eV emissions. All three display high intensity primarily in three spatial regions. Interestingly, these high carrier concentration regions appear to extend along columns a significant distance from the interface. We attribute the 3.41 eV emission to an exciton bound to stacking faults.[25] Significantly, the 3.30 eV emission related to cubic zinc-blende phase GaN appears in almost the same regions as the 3.41 eV emission. This is not surprising since stacking faults are known to give rise to zinc-blende GaN. It appears from Fig. 12 that such new phase formation is associated with highly doped areas. The short-range order of wurtzite and zinc-blende GaN structures is virtually identical, however, the stacking sequence of atom arrangement in closed-packed planes is different, i.e., $\cdots AaBbAaBbAaBb\cdots$ for the wurtzite, and $\cdots AaBbCcAaBbCc\cdots$ for the zinc blende. A fault in the stacking sequence transforms one structure into the other, hence the respective stacking fault energy corresponds to the free energy difference between the wurtzite and zinc-blende modifications. As a consequence, the density of such structural defects is expected to be high in nitrides exhibiting a low energy difference between these phases.[42] Similar phenomena were also observed in cubic GaN.[43] The high defect density may be responsible for the high doping density since O can probably diffuse more rapidly in highly defective regions.

VI. DISCUSSION

Depth-dependent CLS and CL images provide new information for detecting the location and physical origin of defects and impurity doping at GaN/Al_2O_3 interfaces. Temperature-dependent CLS also aid in identifying the various transitions observed in GaN epilayers grown on sapphire substrates. Impurity state densities depend strongly on substrate chemical and thermal treatments. Figure 13 shows CL spectra of three samples (A_2: 5 μm, B: 11 μm, and C: 17 μm) (a) near interface and (b) at bulk regions. The d_{int} for each spectrum is indicated in the figure. As shown in Fig. 13(b), all three samples that we investigated at low temperature display strong donor bound exciton emission in bulk regions at 10 K. We show the depth-profile CLS of these three samples in Figs. 3, 7, and 11. The FWHM values of the D^0X transitions become narrower as the samples get thicker, indicative of improved crystal quality. Such variations reflect the material's inhomogeneity, which is common for GaN epilayers on sapphire. Free excitons were observed in both sample A_2 and B, but not in sample C, indicative of higher quality in the former. This finding is in good agreement with ECV results. As indicated in Fig. 13, n_{int} increases with increasing specimen thickness. As Figs. 13(a) and 13(b) show, FERB can be only observed near the interface region in samples A_2 and B, which have lower sheet carrier concentration and are thinner. However, in sample C, the emission from FERB increases and extends further into the bulk re-

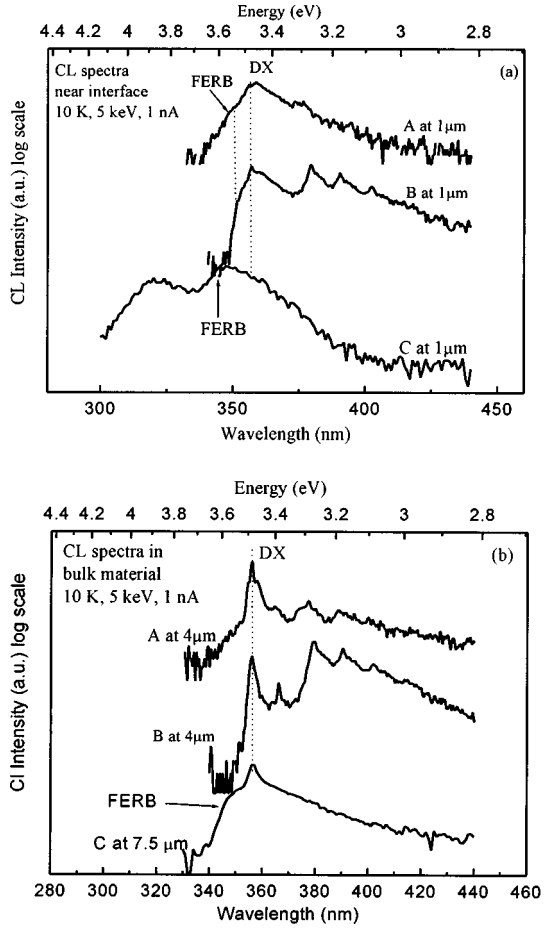

FIG. 13. HVPE GaN/Al_2O_3 CL near-interface spectra. Band tailing, band filling, and possible alloying are evident at higher sheet carrier concentration.

gion. It indicates that impurity diffusion for thicker specimens may extend further from the interface, i.e., to $d_{\text{int}} > 10\ \mu$m for sample C. Such extended impurity diffusion is most evident for this thickest sample (C), consistent with its longest time at elevated growth temperature.

We observe various optical transitions related to defects, impurities, and a secondary phase in the cross section of each sample. Sample A_2, with a ZnO buffer layer, has lower sheet carrier concentration, displaying weak residual acceptor related luminescence. The residual acceptor can either be Zn or C. This sample also shows excitonic emission bound to stacking faults and cubic phase GaN. There is no evidence showing the formation of Al–N–O near the interface in this sample. However, in a 70-μm sample (A_1), grown under similar growth conditions as those of A_2, a broad emission was observed well above the band edge at 3.8 eV at room temperature near the interface. We argue that this is due to a defect complex, analogous to the O impurity in AlN.[39] Differences in the 3.8 eV emission intensities may be due to different times at elevated growth temperatures, during which Al, O, and N interdiffusion could occur. Since growth rates are comparable, thicker samples held at elevated temperatures the longest might be expected to exhibit such diffusion the most. The 3.8 eV peak emission intensity for specimen C relative to those of A and B is consistent with this trend, although the limited data here preclude any general correlation.

The sample with medium n_{int} (sample B) shows strong emissions attributed to residual acceptors. The acceptor can be due either to C or the Ga vacancy, since there is no Zn or Mg found by SIMS. A new donor level at 3.447 eV appears at the GaN/sapphire interfaces whose energy and spatial extent correlate strongly with O outdiffusion. The intensity of this peak is in good agreement with the O distribution, as evidenced by SIMS. Our results show that the source of O is the Al_2O_3 substrate since the O distribution is highest near the interface. Oxygen, not necessarily localized in the interface region, can also be due to the growth environment since a high acceptor density is also observed in this sample.

Sample C displays a large-scale columnar structure, in agreement with the observations of Paskova *et al.*[22] The NBE emission quenches near the interface and grain boundaries where very high defect densities appear. A broad emission band at 3.56 eV likely due to FERB was observed, showing high degenerate doping near interface and grain boundaries. Al–N bonding is not unexpected, given the O release from Al_2O_3 at the atomic-scale interface.[17] It is not surprising that stacking faults and zinc-blende GaN are formed in these highly doped areas. Together with this degenerate doping, Al–N–O complexes form near the interface of this high N_{int} sample as well.

VII. CONCLUSIONS

CL imaging and temperature-dependent CLS show systematic variations in defect emissions with a wide range of HVPE GaN/sapphire electronic properties. We report large differences between interface and bulk in terms of band edge and deep level emission. These emissions correspond to regions of high carrier concentration, impurity doping, and new phase formation. We observe interface features indicating a new donor level involving O impurities that can account for SIMS and ECV results. Highly degenerate interface regions give rise to above band-gap emissions due to band filling and possible alloy formation. Combined with the cross sectional SEM and CL images of the defects, the spatial data provide new information on the nature of impurity diffusion and doping at the GaN/Al_2O_3 interface.

ACKNOWLEDGMENTS

This work was supported by the Office of Naval Research, the National Science Foundation, the Air Force Office of Scientific Research, and the Department of Energy (depth-dependent measurements). The authors thank Dr. T. Paskova (Linköping University) and Dr. R. Vaudo (ATMI) for samples, as well as Dr. S. Mitha and Dr. S. Novak (Chas. Evans and Associates) for SIMS profiles. The Lincoln Laboratory portion of this work was sponsored by the Office of Naval Research under Air Force Contact No. F19628-00-C-0002. Opinions, interpretations, conclusions, and recommendations are those of the authors and are not necessarily endorsed by the United States Air Force.

[1] S. Nakamura and G. Fasol, *The Blue Laser Diode* (Springer, Berlin, 1997).
[2] M. Razeghi and A. Rogalski, J. Appl. Phys. **79**, 7433 (1997).
[3] J. Y. Duboz and M. A. Khan, in *Group III Nitride Semiconductor Compounds*, edited by B. Gil (Clarendon, Oxford, 1998), p. 343.
[4] H. P. Maruska and J. J. Tietjen, Appl. Phys. Lett. **15**, 327 (1969).
[5] C. R. Miskys, M. K. Kelly, O. Ambacher, G. Martínez-Criado, and M. Stutzmann, Appl. Phys. Lett. **77**, 1858 (2000).
[6] S. Fisher, C. Wetzel, E. E. Haller, and B. K. Meyer, Appl. Phys. Lett. **67**, 1298 (1995).
[7] M. A. L. Johnson, Z. Yu, C. Boney, W. C. Hughes, J. W. Cook, J. F. Schetzina, H. Zhao, B. J. Skromme, and J. A. Edmond, Mater. Res. Soc. Symp. Proc. **449**, 215 (1997).
[8] B. Monemar, J. Cryst. Growth **189/190**, 1 (1998).
[9] W. Götz, J. Walker, L. T. Romano, N. M. Johnson, and R. J. Molnar, Mater. Res. Soc. Symp. Proc. **449**, 525 (1997).
[10] D. C. Look and R. J. Molnar, Appl. Phys. Lett. **70**, 3377 (1997).
[11] X. L. Xu, C. D. Beling, S. Fung, Y. W. Zhao, N. F. Sun, T. N. Sun, Q. L. Zhang, H. H. Zhan, B. Q. Sun, J. N. Wang, W. K. Ge, and P. C. Wong, Appl. Phys. Lett. **76**, 152 (2000).
[12] G. Popovici, W. Kim, A. Botchkarev, H. Tang, H. Morkoc, and J. Solomon, Appl. Phys. Lett. **71**, 3385 (1997).
[13] J. E. Van Nostrand, J. Solomon, A. Saxler, Q.-H. Xie, D. C. Reynolds, and D. C. Look, J. Appl. Phys. **87**, 8766 (2000).
[14] L. T. Romano, B. S. Krusor, and R. J. Molnar, Appl. Phys. Lett. **71**, 2283 (1997).
[15] S. H. Goss, A. P. Young, and L. J. Brillson, Mater. Res. Soc. Symp. Proc. **639**, G3.59.1 (2001).
[16] M. Godlewski, E. M. Goldys, M. R. Phillips, R. Langer, and A. Barski, Appl. Phys. Lett. **73**, 3686 (1998).
[17] R. A. Youngman and J. H. Harris, J. Am. Ceram. Soc. **73**, 3238 (1990).
[18] J. I. Pankove and J. A. Hutchby, J. Appl. Phys. **47**, 5387 (1976).
[19] S. Gu, R. Zhang, J. Sun, L. Zhang, and T. F. Kuech, Appl. Phys. Lett. **76**, 3454 (2000).
[20] K. Fleischer, M. Toth, M. R. Phillips, J. Zou, G. Li, and S. J. Chua, Appl. Phys. Lett. **74**, 1114 (1999).
[21] H. C. Yang, T. Y. Lin, and Y. F. Chen, Phys. Rev. B **62**, 12593 (2000), and references therein.
[22] T. Paskova, E. M. Goldys, R. Yakimova, E. B. Svedberg, A. Henry, and B. Monemar, J. Cryst. Growth **208**, 18 (2000).
[23] B. J. Skromme, J. Jayapalan, R. P. Vaudo, and V. M. Phanse, Appl. Phys. Lett. **74**, 2358 (1999).
[24] B. Meyer, Mater. Res. Soc. Symp. Proc. **449**, 497 (1997).
[25] M. Albrecht, S. Christiansen, G. Salviati, C. Zanotti-Fregonara, Y. T. Rebane, Y. G. Shreter, M. Mayer, A. Pelzmann, M. Kamp, K. J. Ebeling, M. D. Bremser, R. F. Davis, and H. P. Strunk, Mater. Res. Soc. Symp. Proc. **468**, 293 (1997).
[26] N. Grandjean, M. Leroux, M. Laügt, and J. Massies, Appl. Phys. Lett. **71**, 240 (1997).
[27] S. Fischer, G. Steude, D. M. Hofmann, F. Kurth, F. Anders, M. Topf, B. K. Meyer, F. Bertram, M. Schmidt, J. Christen, L. Eckey, J. Holst, A. Hoffmann, B. Mensching, and B. Rauschenbach, J. Cryst. Growth **189/190**, 556 (1998).
[28] S. Fischer, C. Wetzel, W. Walukiewicz, and E. E. Haller, Mater. Res. Soc. Symp. Proc. **395**, 571 (1996).
[29] E. Calleja, M. A. Sanchez-Garcia, F. J. Sanchex, F. Calle, F. B. Naranjo, E. Munoz, Y. Jahn, and K. Ploog, Phys. Rev. B **62**, 16826 (2000).
[30] M. Leroux, N. Grandjean, B. Beaumont, G. Nataf, F. Semond, J. Massies, and P. Gibart, J. Appl. Phys. **86**, 3721 (1999).
[31] H. Siegle, A. Hoffmann, L. Eckey, and Thomsen, Appl. Phys. Lett. **71**, 2490 (1997).
[32] B. K. Meyer, D. Volm, A. Graber, H. C. Alt, T. Detchprohm, A. Amano, and I. Akasaki, Solid State Commun. **95**, 597 (1995).
[33] Chas. Evans and Associates, 810 Kaifer Road, Sunnyvale, CA 94086.
[34] D. C. Look, C. E. Stutz, R. J. Molnar, K. Saarinen, and Z. Liliental-Weber, Solid State Commun. **117**, 571 (2001).
[35] D. Volm, K. Oettinger, T. Streibl, D. Kovalev, M. Ben-Choriin, J. Diener, B. K. Meyer, J. Majewski, L. Eckey, A. Hoffmann, H. Amano, I. Akasaki, K. Hiramatsu, and T. Detchprohm, Phys. Rev. B **53**, 16543 (1996).
[36] K. Saarinen, T. Laine, S. Kuisma, J. Nissilä, P. Hautojärvi, L. Dobrzynski, J. M. Baranowski, K. Pakula, R. Stepniewski, M. Wojdak, A. Wysmolek, T. Suski, M. Leszczynski, I. Grzegory, and S. Porowski, Phys. Rev. Lett. **79**, 3030 (1997).
[37] B. Monemar, J. Mater. Sci.: Mater. Electron. **10**, 227 (1999); W. J. Moore, J. A. Freitas, Jr., and R. J. Molnar, Phys. Rev. B **56**, 12073 (1997).
[38] B. Arnaudov, T. Paskova, E. M. Goldys, R. Yakimova, S. Evtimova, I. G. Ivanov, A. Henry, and B. Monemar, J. Appl. Phys. **85**, 7888 (1999).
[39] A. P. Young, J. Schäfer, L. J. Brillson, Y. Yang, S. H. Xu, H. Cruguel, G. J. Lapeyre, M. A. L. Johnson, and J. F. Schetzina, J. Electron. Mater. **28**, 308 (1999).
[40] K. Uchida, A. Watanabe, F. Yano, M. Kouguchi, T. Tanaka, and S. Minagawa, J. Appl. Phys. **79**, 3487 (1996).
[41] M. Seelmann-Eggebert, H. Zimmermann, H. Obloh, R. Niebuhr, and B. Wachtendorf, Mater. Res. Soc. Symp. Proc. **468**, 193 (1997).
[42] J. I. Pankove, *Gallium Nitride I* (Academic, San Diego, 1998).
[43] X. L. Sun, H. Yang, L. X. Zheng, D. P. Xu, J. B. Li, Y. T. Wang, G. H. Li, and Z. G. Wang, Appl. Phys. Lett. **74**, 2827 (1999).